

## Direct-write bioprinting of cell-laden methacrylated gelatin hydrogels

This content has been downloaded from IOPscience. Please scroll down to see the full text.

View [the table of contents for this issue](#), or go to the [journal homepage](#) for more

Download details:

IP Address: 193.137.16.117

This content was downloaded on 25/06/2015 at 10:47

Please note that [terms and conditions apply](#).

# Direct-write bioprinting of cell-laden methacrylated gelatin hydrogels

Luiz E Bertassoni<sup>1,2,3</sup>, Juliana C Cardoso<sup>2,3,4</sup>, Vijayan Manoharan<sup>2,3,5</sup>, Ana L Cristino<sup>2,3</sup>, Nupura S Bhise<sup>2,3</sup>, Wesleyan A Araujo<sup>2,3</sup>, Pinar Zorlutuna<sup>2,3,9</sup>, Nihal E Vrana<sup>2,3</sup>, Amir M Ghaemmaghami<sup>6</sup>, Mehmet R Dokmeci<sup>2,3,7,8</sup> and Ali Khademhosseini<sup>2,3,7,8</sup>

<sup>1</sup> Biomaterials Research Unit, Faculty of Dentistry, University of Sydney, Sydney, NSW 2010, Australia

<sup>2</sup> Center for Biomedical Engineering, Department of Medicine, Brigham and Women's Hospital, Harvard Medical School, Boston, MA 02139, USA

<sup>3</sup> Harvard-MIT Division of Health Sciences and Technology, Massachusetts Institute of Technology, Cambridge, MA 02139, USA

<sup>4</sup> Institute of Technology and Research (LBMAT), Tiradentes University, Aracaju, SE 49032, Brazil

<sup>5</sup> Center for Nanotechnology and Advanced Biomaterials (CeNTAB), SASTRA University, Thanjavur, TN 613401 India

<sup>6</sup> Faculty of Medicine and Health Sciences, University of Nottingham, Nottingham, UK

<sup>7</sup> Wyss Institute for Biologically Inspired Engineering, Harvard University, Boston, MA 02115, USA

E-mail: [alik@rics.bwh.harvard.edu](mailto:alik@rics.bwh.harvard.edu) and [mdokmeci@rics.bwh.harvard.edu](mailto:mdokmeci@rics.bwh.harvard.edu)

Received 3 August 2013, revised 21 October 2013


Accepted for publication 25 November 2013

Published 3 April 2014

## Abstract

Fabrication of three dimensional (3D) organoids with controlled microarchitectures has been shown to enhance tissue functionality. Bioprinting can be used to precisely position cells and cell-laden materials to generate controlled tissue architecture. Therefore, it represents an exciting alternative for organ fabrication. Despite the rapid progress in the field, the development of printing processes that can be used to fabricate macroscale tissue constructs from ECM-derived hydrogels has remained a challenge. Here we report a strategy for bioprinting of photolabile cell-laden methacrylated gelatin (GelMA) hydrogels. We bioprinted cell-laden GelMA at concentrations ranging from 7 to 15% with varying cell densities and found a direct correlation between printability and the hydrogel mechanical properties. Furthermore, encapsulated HepG2 cells preserved cell viability for at least eight days following the bioprinting process. In summary, this work presents a strategy for direct-write bioprinting of a cell-laden photolabile ECM-derived hydrogel, which may find widespread application for tissue engineering, organ printing and the development of 3D drug discovery platforms.

Keywords: bioprinting, hydrogels, GelMA, direct-write, tissue engineering

 Online supplementary data available from [stacks.iop.org/BF/6/024105/mmedia](http://stacks.iop.org/BF/6/024105/mmedia)

(Some figures may appear in colour only in the online journal)

## 1. Introduction

Due to a growing need for organ transplantation and a short supply of donor organs, tissue engineering has progressed

rapidly toward the development of new technologies for organ fabrication [1]. Although a few exciting clinical outcomes have been obtained in engineering relatively simple scaffolds seeded with autologous cells [2–6], improved methods for fabrication of cell-laden constructs with greater complexity are still under investigation [6]. Due to the ability to pattern biomaterials with micrometer precision in three dimensions (3D), bioprinting

<sup>8</sup> Authors to whom any correspondence should be addressed.

<sup>9</sup> Biomedical Engineering Program and Mechanical Engineering Department, University of Connecticut, 191 Auditorium Road, Storrs, CT 06269–3139, USA.

represents an appealing alternative to address these growing requirements in biomedical engineering [7].

Bioprinting allows for the precise positioning of cellularized structures on demand, either embedded in hydrogels or free from scaffold support [7]. The concept of bioprinting stems from the additive manufacturing philosophy, where the sequential deposition of solid layers creates 3D objects. Several types of bioprinting systems have been described in the literature. In inkjet bioprinting, for instance, a container, analogue to ink-cartridges, dispenses drops in the range of 1 to 100 pl via heating and vaporizing, while either a bubble or a piezoelectric actuator forces the liquid drop toward a supporting substrate [8]. In common laser bioprinters, on the other hand, a high-energy pulsed laser beam transfers a biomaterial containing cells, proteins or growth factors of interest to an underlying substrate, via a mechanism known as laser-induced forward-transfer technique [9, 10]. Direct-write bioprinters, in turn, generally promote the extrusion of a viscous polymer precursor to build up a tissue layer [11].

While a variety of strategies have been established to bioprint hydrogels as a seeding substrate upon which cells can proliferate [7, 12–17], methods for bioprinting naturally derived cell-laden hydrogels are still limited [7]. Interesting tissue engineering alternatives have been reported for inkjet printing of natural proteins and polysaccharides, such as agar [18], fibrin [16], Ficoll [19], hyaluronic acid [15], gelatin [15], collagen [11] and blends of these materials [20, 21]. However, direct-write bioprinting of cell-laden ECM-derived hydrogels has remained a challenge. For instance, bioprinting of a hydrogel constituted of a blend of methacrylated ethanolamide gelatin and methacrylated hyaluronic acid has been recently reported [15]. However, this complex process required multiple photopolymerization steps both before (3 min) and after (2 min) printing, respectively to control hydrogel viscosity and to form a stable construct after printing. Furthermore, the range of hydrogel concentrations allowing for gel extrusion was highly restricted, which has been a common limitation for bioprinting of viscous polymers from a nozzle or syringe.

Herein, we propose an alternative strategy for direct-write bioprinting of a cell-laden ECM-derived methacrylated gelatin (GelMA) hydrogel [22] at a wide range of concentrations, mechanical properties and cell densities, while preserving high cell viability [23, 24]. In our method, a commercially available bioprinter (Organovo) was modified to dispense pre-polymerized cell-laden GelMA hydrogel fibers. This overcomes the limitations associated with dispensing viscous polymers, such as nozzle clogging and restricted concentrations allowing for gel extrusion. Ultimately, we envision that the proposed method may be utilized to fabricate 3D constructs that replicate the function of native tissues. To this end, we utilized hepatocyte- and fibroblast-laden GelMA hydrogels as a model to demonstrate the feasibility of the proposed technique in bioprinting constructs with preserved cell viability over time.

## 2. Materials and methods

### 2.1. Methacrylated gelatin hydrogel synthesis

GelMA was synthesized as described previously [19]. Briefly, 10% (w/v) type A gelatin derived from porcine skin (Sigma-Aldrich) was dissolved into Dulbecco's phosphate buffered saline (DPBS; GIBCO) by stirring at 60 °C. Methacrylic anhydride (Sigma-Aldrich) was added drop-wise to the solution at a rate of 0.5 mL min<sup>-1</sup> and allowed to react for 3 h at 50 °C. Following a 5 × dilution with addition of DPBS at 40 °C, the mixture was dialyzed against deionized water using a dialysis tubing (12–14 kDa cutoff) for seven days at 40 °C. The solution was lyophilized for 3–4 days to generate a white porous foam and stored at –80 °C until further use. Freeze dried GelMA macromers were mixed at concentrations of 5, 7, 10 and 15% (w/v) into DPBS containing 0.5% (w/v) photoinitiator (2-hydroxy-1-(4-(hydroxyethoxy)phenyl)-2-methyl-1-propanone; Irgacure 2959, CIBA Chemicals).

### 2.2. Bioprinting process

A modified NovoGen MMX Bioprinter™ (Organovo) was used for the experiments in this work (figure 1(a)). The bioprinter is composed of two pumps and two nozzles assembled in a motor-driven X–Z robot, where one is specifically designed to aspirate and dispense cells, whereas the other aspirates and dispenses hydrogels. An additional motorized stage moving in the Y direction controls the position of the printed material in coordination with the X–Z robot. Although this system was originally developed to bioprint cells and hydrogels separately, here we modified it to bioprint cells encapsulated in the GelMA hydrogel in a single step. A UV light guide (Omniscure S2000) was added to the bioprinter to allow photopolymerization of the hydrogel precursor inside the capillary after aspiration. In brief, the hydrogel 'ink' is bioprinted by following the steps illustrated in figure 1. Firstly, the cell-laden hydrogel precursor is aspirated by immersing a 500 μm internal diameter and 85 mm long glass capillary in a hydrogel vial (figure 1(b)). The glass capillary contains a motorized internal metallic piston, which moves in the Z direction. Secondly, the hydrogel precursor is aspirated by the upward movement of the metallic piston. Next, the cell-laden precursor is photocrosslinked under 6.9 mW cm<sup>-2</sup> of UV light (360–480 nm) for 10, 15, 30 or 60 s (figure 1(c)). After photopolymerization, the metallic piston is pushed down against the crosslinked hydrogel, while a custom script controls the dispense speed and the coordinated movement of the motorized X–Z robot and Y stage (figure 1(d)).

### 2.3. Cell culture

Immortalized HepG2 and NIH3T3 cells were obtained from ATCC. The culture medium for all experiments was Dulbecco's modified Eagle medium (DMEM, Gibco) supplemented with 10% fetal bovine serum and 1% penicillin–streptomycin. Cells were cultured on tissue culture plates (Corning Incorporated) and maintained at 37 °C in a

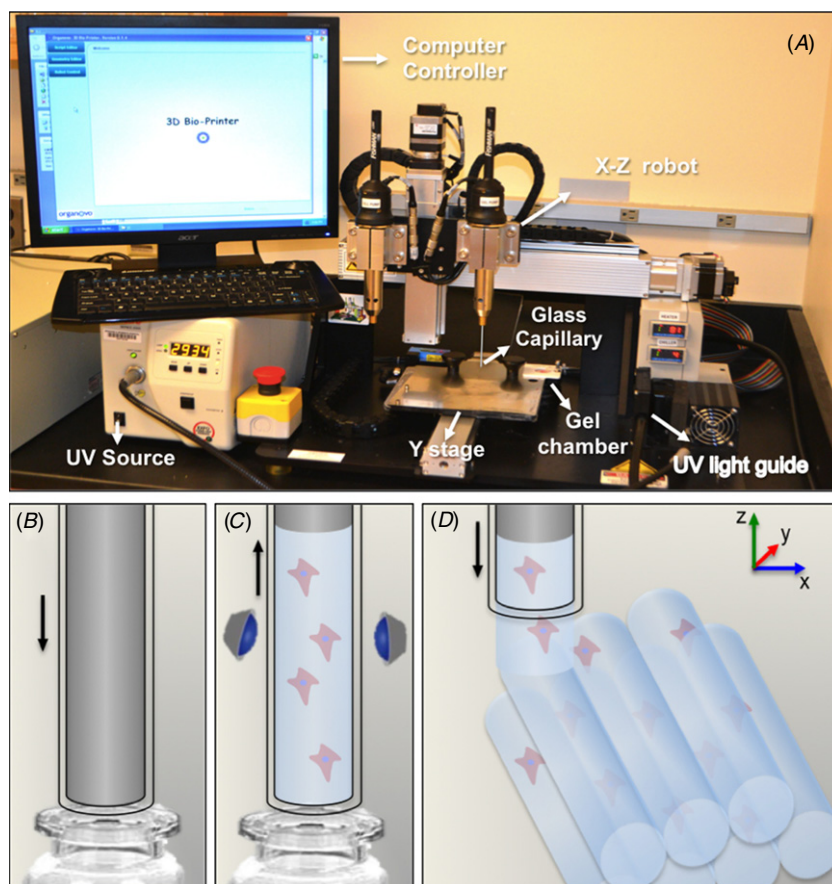


**Figure 1.** Bioprinter setup for direct-write printing of cell-laden GelMA hydrogels. (A) Photograph of NovoGen MMX Bioprinter™ (Organovo) showing the gel and cell-dispensing capillaries mounted on an X–Z motorized stage. (B) To print the hydrogel fibers, a metallic piston fitted inside a glass capillary is immersed in a vial containing the cells and the hydrogel precursor. (C) The upward movement of the metallic piston aspirates the cell-laden hydrogel precursor, which is subsequently crosslinked by exposure to light. (D) Next, the coordinated motion of the motorized stage enables precise printing of cell-laden GelMA hydrogel fibers.

humidified atmosphere with 5% of CO<sub>2</sub>. The media was changed three times per week and the cells were passaged once per week.

#### 2.4. Printability of GelMA hydrogels

A printability assay was performed to determine the reproducibility of the printing process for hydrogels with different concentrations and exposure times. Firstly, GelMA hydrogel precursors with concentrations ranging from 5 to 15% (w/v) were aspirated into the glass capillary to dispense 30 mm fibers and photocrosslinked from 10 to 60 s. The gelled fibers were subsequently printed at a dispense speed of 2 mm s<sup>-1</sup>. Printing was deemed successful if all of the dispensed lines ( $n = 9$ ) were extruded with a preserved cylindrical shape at the expected architecture that replicated the shape of the glass capillary. To evaluate the printability of cell-laden GelMA hydrogels relative to UV exposure times and cell concentrations, we selected 10% GelMA encapsulated with cell concentrations of  $1 \times 10^6$ ,  $1.5 \times 10^6$ ,  $3 \times 10^6$ , and  $6 \times 10^6$  cells mL<sup>-1</sup>. The cell-laden hydrogel precursors were aspirated into the glass capillary and photocrosslinked from 10 to 60 s ( $n = 9$ ). The same parameters described above were adopted to determine successful printing.

#### 2.5. Mechanical properties

The elastic modulus of the hydrogels was determined to investigate the correlation between hydrogel mechanical properties and printability. Mechanical tests were performed following protocols described previously [22]. For each sample, eighty microliters of cell-free, 5 to 15% (w/v) GelMA hydrogel precursor was pipetted in a pre-fabricated circular PDMS mold measuring 8 mm in diameter and 1 mm in thickness. The hydrogel precursors were exposed to 6.9 mW cm<sup>-2</sup> UV light (360–480 nm) from 10 to 60 s (Omnigene S2000). Samples were retrieved from the molds and incubated in DPBS at room temperature for 24 h. Prior to testing, the discs were blot dried and tested with a cross-head speed of 0.1 mm min<sup>-1</sup> on an Instron 5542 universal mechanical testing machine. The compressive modulus was determined as the slope of the linear region corresponding to 0–10% strain.

#### 2.6. Interfacial properties of GelMA hydrogels during bioprinting

Interfacial properties were determined to investigate whether the load required to dispense the hydrogel fibers from the

glass capillaries was associated with reproducible printing. Assuming the crosslinked hydrogel as a fiber of known geometry embedded in a frictionless capillary, we determined the maximum load required to debond the hydrogel from the glass surface, which is associated with the stress required to initiate dispensing. For each measurement, 20 mm of hydrogel precursor (5 to 15% w/v) was aspirated into the glass capillary and photocrosslinked from 10 to 60 s. A mechanical testing machine (Instron 5542) equipped with a metallic piston with the same dimensions to the ones used in the bioprinter was used to extrude the hydrogel out of the glass capillary at a rate of  $2 \text{ mm s}^{-1}$ , similar to the rate used for bioprinting ( $n = 6$ ). The changes in load versus displacement were recorded and the peak in load was used to determine the average maximum load at debonding, which is consistent with the load required to initiate dispensing of the hydrogel fibers from the glass capillary. Both cell-free and cell-laden ( $1 \times 10^6$  and  $5 \times 10^6 \text{ cells mL}^{-1}$ ) gels were tested.

### 2.7. Bioprinting of varying architectures using cell-laden GelMA hydrogels

To demonstrate the versatility of the proposed method to fabricate cell-laden GelMA hydrogel constructs with different designs, we bioprinted 3D lattice constructs on TMSPMA treated glass by dispensing Z-stacked perpendicular fibers of 10% (w/v) GelMA hydrogels encapsulated with  $1.5 \times 10^6$  HepG2 cells  $\text{mL}^{-1}$ . Constructs with stacked parallel GelMA fibers encapsulated with  $1.5 \times 10^6$  NIH3T3 cells  $\text{mL}^{-1}$  were also bioprinted, and cell viability was determined by using a live/dead assay kit (Invitrogen) as described below. Stability of the lattice and stacked-fiber constructs was warranted by dispensing a droplet ( $5 \mu\text{l}$ ) of hydrogel precursor over the printed construct and exposing it to secondary photocrosslinking step of 5 s. Microchannels were fabricated by alternating the printing of cell-laden GelMA hydrogel fibers and cell-free agarose fibers, which were subsequently removed. To demonstrate the versatility of the printing method, a bioprinted HepG2-laden hydrogel microarray was also fabricated by dispensing  $0.5 \mu\text{l}$  drops of hydrogel precursors and subsequently exposing them to UV light using the same parameters to induce photocrosslinking as described above. Additionally, GelMA was loaded with 1% (v/v) fluorescent microbeads, bioprinted to replicate the MIT logo and imaged under UV light to highlight the morphology of the printed fibers. Finally, hollow fibers were formed by aspirating the hydrogel precursor in adapted 1 mm capillaries with a  $250 \mu\text{m}$  piston located inside it, photocrosslinking the gel, and dispensing the final crosslinked structure.

To visualize the morphology of the encapsulated cells in bioprinted GelMA hydrogels, constructs were stained with Rhodamine-Phalloidin (Alexa-Fluor 594; Invitrogen) and 40,6-diamidino-2-phenylindole (DAPI; Sigma). The constructs were first fixed in 4% (v/v) paraformaldehyde (Electron Sciences) solution in PBS for 30 min. To stain F-actin filaments, cell-laden gels were permeabilized in 0.1% (w/v) Triton X-100 solution in PBS for 20 min and blocked in 1% (w/v) bovine serum albumin (BSA) for 1 h. The samples were then incubated in a 1:40 ratio solution of Alexa Fluor-594

Phalloidin in 0.1% BSA for 45 min at room temperature. The samples were then incubated in 0.1% (v/v) DAPI solution in PBS for 10 min at  $37^\circ\text{C}$  to stain the cell nuclei. The stained samples were then washed twice with PBS before imaging with a fluorescence microscope (Nikon TE 2000-U).

### 2.8. Cell viability assay

Cell viability was determined by using a live/dead assay kit (Invitrogen) according to the manufacturer's instructions. In this protocol, live cells were stained with calcein AM (green) and dead cells with ethidium homodimer-1 (red). After 20 min of incubation at  $37^\circ\text{C}$  the live and dead cells were observed using an inverted fluorescence microscope (Nikon TE 2000-U). The number of live and dead cells was counted by ImageJ software using at least four images from different areas of three bioprinted structures for each condition. Cell viability was then calculated based on the percentage of live cells to total cells in the construct. As a control,  $5 \mu\text{l}$  of cell-laden 10% GelMA was dispensed on a flat surface between two fixed glass cover slips. A TMSPMA coated glass was then positioned on top of the hydrogel precursor and the entire assembly was photocrosslinked following the protocol described above.

### 2.9. Statistical analysis

Statistical analysis was performed using GraphPad Prism 6. All of the data is presented as the mean  $\pm$  standard deviation. A comparison of values was carried out by one-way/two-way analysis of variance (ANOVA) and Tukey post-hoc test. Statistically significant values are presented as  $*p < 0.05$ ,  $**p < 0.01$ ,  $***p < 0.001$  and  $****p < 0.0001$ .

## 3. Results and discussion

### 3.1. Printability of GelMA hydrogels

The primary objective of this work was to develop a strategy to bioprint cell-laden GelMA hydrogels. To achieve this objective we developed a modified bioprinting set-up that could be utilized to fabricate 3D microarchitectures of pre-polymerized cell-laden GelMA while preserving high cell viability.

We initially optimized the bioprinting process by assessing the printability of GelMA hydrogels as a function of concentration and UV exposure times. Earlier reports suggest that GelMA hydrogels with concentrations ranging from 5 to 15% can support cell spreading, proliferation and metabolism [22, 25, 26]. Furthermore, UV light exposures for at least 60 s did not visibly influence the viability of cell-laden GelMA hydrogels [22]. In agreement with these results, our experiments suggest that GelMA hydrogels may be successfully bioprinted at concentrations ranging from 7 to 15%, for all UV exposure times tested (figure 2(a)). Interestingly, we observed that at lower concentrations, hydrogels were not easily printed to generate uniform and well-structured fibers (figure 2(a)). We then selected 10% GelMA to test the effect of cell density on the printability of cell-laden gels. Results demonstrated that lower UV light exposure times consistently reduced printability (figure 2(b)).

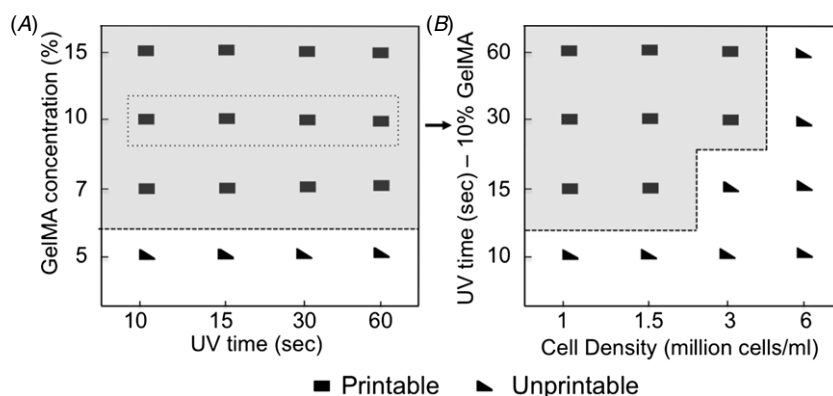


**Figure 2.** Printability of GelMA hydrogels as a function of concentration, UV light exposure time, and cell density. (A) Printability of cell-free GelMA hydrogels at concentrations ranging from 5 to 15%, photocrosslinked from 10 to 60 s. (B) Printability of 10% HepG2-laden GelMA, photocrosslinked from 10 to 60 s ( $n = 9$ ).

Similarly, an increase in cell density from  $1 \times 10^6$  to  $6 \times 10^6$  cells  $\text{mL}^{-1}$  affected the reproducibility of bioprinting. Despite the restrictions encountered for higher cell densities, a wide range of hydrogel concentrations and UV light exposure times enabled reproducible bioprinting.

To further characterize the effect of mechanical properties on the success of GelMA hydrogel bioprinting, we measured the elastic modulus of the hydrogels in all conditions tested. Consistent with results reported earlier [22, 26, 27], we found that the elastic modulus of the hydrogels increased proportionally with an increase in polymer concentration and UV light exposure times (figure 3(a)). Accordingly, 15% GelMA hydrogels had the highest elastic modulus and showed a more significant modulus increase in response to longer exposure to UV light (figure 3(b)). For this group we observed an increase from  $2.6 \pm 0.6$  kPa, at 10 s of light exposure, to  $60.3 \pm 9.5$  kPa, at 60 s ( $p < 0.0001$ ). The effect of UV light exposure decreased gradually for 10 and 7% GelMA hydrogel concentrations, where the lowest and highest moduli were  $2.4 \pm 0.4$  and  $19.0 \pm 3.5$  kPa for 7% hydrogels, and  $1.2 \pm 0.1$  and  $6.5 \pm 0.8$  kPa for 10% hydrogels, respectively. Considering the hydrogel elastic modulus as a reference value for printability, our results show that while hydrogels with modulus below 1 kPa were unprintable, gels with elastic modulus ranging from  $1.2 \pm 0.1$  kPa up to  $2.6 \pm 0.6$  kPa had variable printability, and gels with modulus above 2.6 kPa were reproducibly printed. These results, combined with our observations for hydrogel printability, shown in figure 2, support the notion that higher stiffness may facilitate direct-write bioprinting of pre-polymerized GelMA hydrogels.

Since the bioprinting method that we developed depends on (1) the aspiration of the hydrogel precursor followed by (2) photocrosslinking inside a glass capillary and (3) dispensing via mechanical extrusion, we hypothesized that interfacial properties of the crosslinked gel relative to the glass capillary could be important for ensuring high quality and reproducible printing. Given that GelMA is primarily constituted of electrostatically charged macromolecules and has intrinsic adhesive properties due to the presence of uncured acrylate groups, we hypothesized that different hydrogel concentrations and UV light exposure times could require different loads to extrude the hydrogel fibers. Therefore,

we analyzed the load versus displacement curves obtained while hydrogels were dispensed from a glass capillary and determined the average peak load during extrusion. To accomplish this, we followed a technique commonly used in the fiber reinforced composite industry [28]. By adapting a system whereby a fiber is impregnated in a polymer matrix, and the maximum load required to initiate debonding is associated with the interfacial properties between fiber and matrix, we considered the hydrogel as a fiber of known cross-sectional area, impregnated in a glass matrix, extruded by a unidirectional force [28]. We then quantified the maximum load required for the piston to debond the hydrogel from the glass capillary and initiate dispensing. Results showed a general increase in maximum load at debonding for higher hydrogel concentrations, where 15% GelMA crosslinked for 60 s yielded the highest average ( $1.52 \pm 0.23$  N), and 5% GelMA crosslinked for 60 s yielded the lowest average ( $0.24 \pm 0.04$  N) (figure 4(b)). Overall, all groups, except 5% GelMA crosslinked for 60 s, were significantly higher than the control, which showed the load associated with piston extrusion from a glass capillary without the hydrogel. Interestingly, an increase in maximum load at debonding was associated with higher printability. Additional analyses to compare the load versus displacement curves of cell-laden GelMA with  $1 \times 10^6$  versus  $6 \times 10^6$  cells  $\text{mL}^{-1}$  revealed no significant differences (figures 5(a) and (b)), thus discounting an association between cell density and interfacial properties. Nevertheless, we observed a trend where the higher cell density tested showed slightly increased maximum load at debonding, which indicates that hydrogels encapsulated with cell concentrations higher than  $6 \times 10^6$  cells  $\text{mL}^{-1}$  may increase the hydrogel debonding stress more significantly. Figure 6 illustrates GelMA hydrogel printability relative to elastic modulus and maximum load at debonding, which may serve as a reference to generalize the proposed approach to other types of gels. Collectively, our results suggest that gels with elastic moduli above  $2.6 \pm 0.1$  kPa and maximum load at debond above  $0.53 \pm 0.1$  N were associated with reproducible printing. To further validate the proposed method using different types of photocrosslinkable hydrogels, we also bioprinted 10% (w/v) poly(ethylene glycol) diacrylate (PEGDA) hydrogels

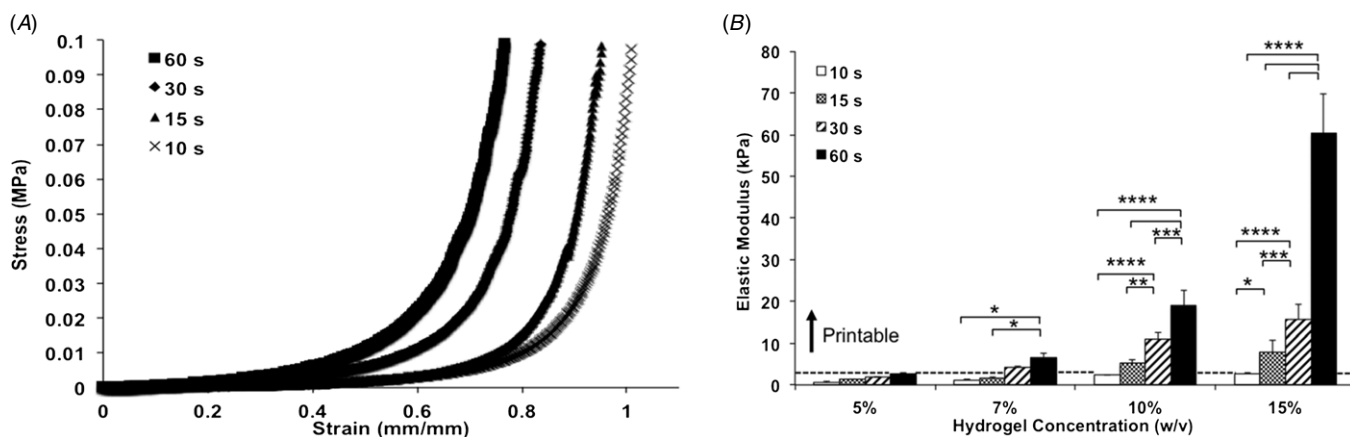


**Figure 3.** Mechanical properties of GelMA hydrogels as a function of concentration and UV light exposure time. (A) Representative stress versus strain curves for 5% GelMA hydrogels at different UV light exposure times. (B) Elastic modulus of GelMA hydrogels increased proportionally with an increase in polymer concentration and UV light exposure time (\* $p < 0.05$ , \*\* $p < 0.01$ , \*\*\* $p < 0.001$  and \*\*\*\* $p < 0.0001$ ). Results suggest that printability is improved for hydrogels presenting higher stiffness, as illustrated by the dashed line representing the lower threshold for successful printing ( $n = 6$ ). (Statistical analyses comparing hydrogels of different concentrations are shown in figure S1 (available from [stacks.iop.org/BF/6/024105/mmedia](http://stacks.iop.org/BF/6/024105/mmedia))).

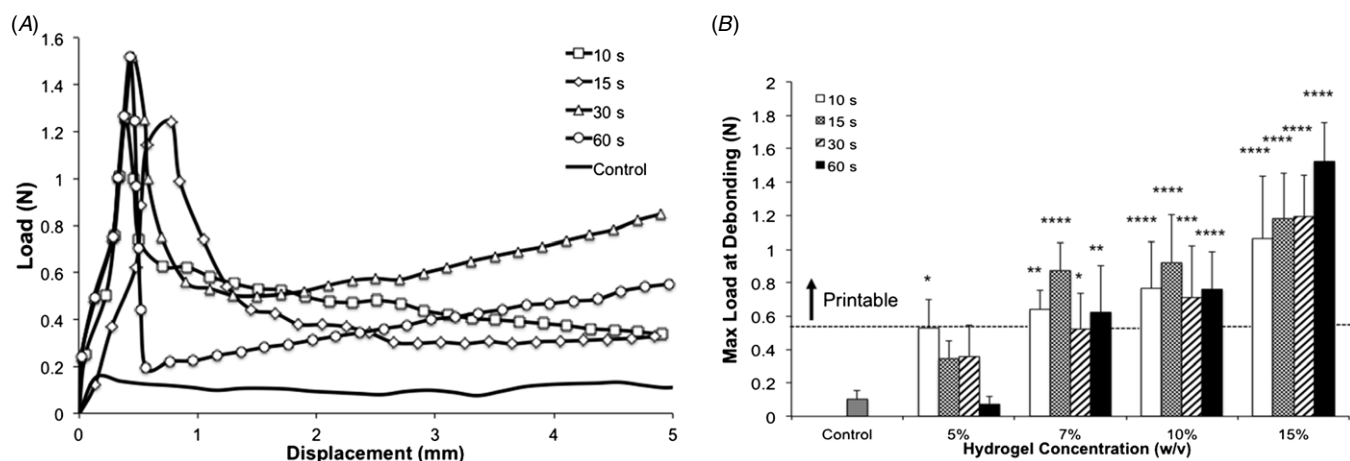


**Figure 4.** Interfacial properties of GelMA hydrogels as extruded from a glass capillary during the bioprinting process. (A) Representative load versus displacement curves for 15% GelMA hydrogels extruded at a rate of  $2 \text{ mm s}^{-1}$ . (B) Maximum load for debonding hydrogels from the glass capillary, representative of force required to initiate bioprinting ( $n = 6$ ). Stars indicate significant difference against the control group (\* $p < 0.05$ , \*\* $p < 0.01$ , \*\*\* $p < 0.001$ , \*\*\*\* $p < 0.0001$ ). The dashed line represents the lower threshold for successful printing. (Statistical analyses comparing the effect of UV light exposure time within hydrogel concentrations are shown in figure S2 (available from [stacks.iop.org/BF/6/024105/mmedia](http://stacks.iop.org/BF/6/024105/mmedia))).

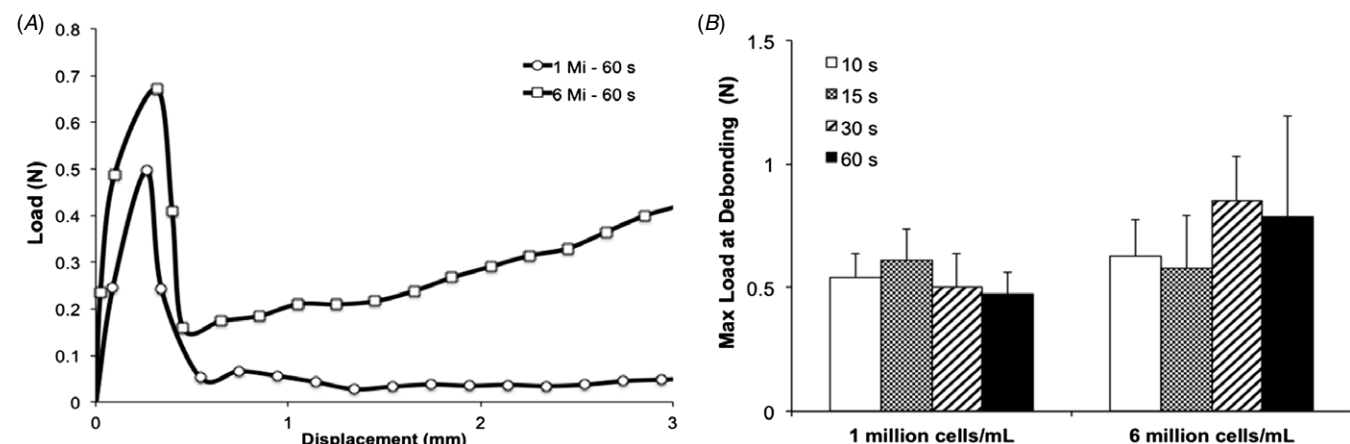


**Figure 5.** Interfacial properties of cell-laden GelMA hydrogels as extruded from a glass capillary during the bioprinting process. (A) Representative load versus displacement curve for cell-laden 10% GelMA hydrogels extruded at a rate of  $2 \text{ mm s}^{-1}$ . (B) Maximum load to debond cell-laden hydrogels from the glass capillary ( $n = 6$ ).

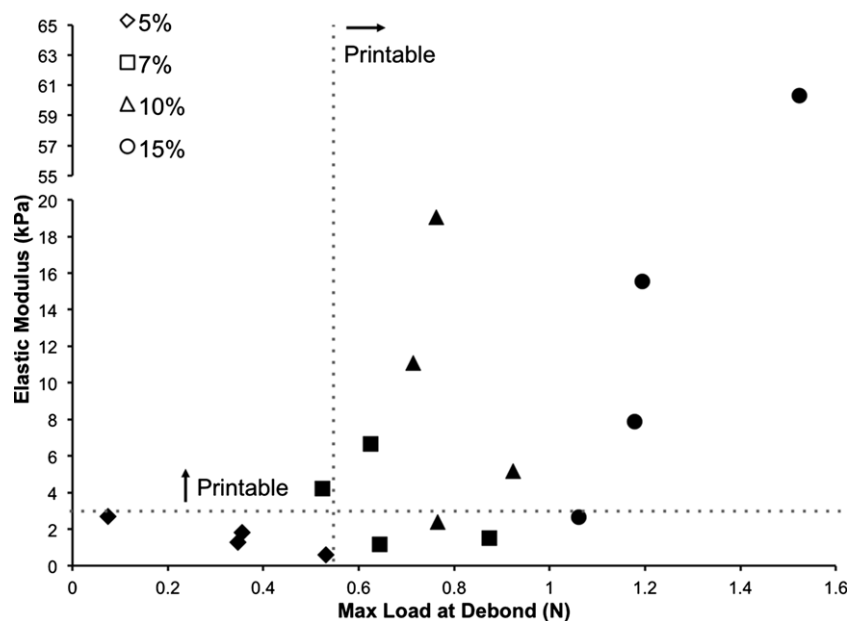


**Figure 6.** Elastic modulus of GelMA hydrogels as a function of maximum load at debond (irrespective of gel concentration and UV light exposure times) representing the respective threshold for consistent printing. Gels with elastic modulus values above 2.6 kPa and maximum load at debond above 0.53 N were reproducibly printed.

and blends of PEGDA with GelMA (figure S4 (available from [stacks.iop.org/BF/6/024105/mmedia](http://stacks.iop.org/BF/6/024105/mmedia))). These gels were all successfully printed, thus confirming the possibility of extending the proposed method to other types of photocrosslinkable cell-laden hydrogels.

In summary, based on the optimization experiments, we selected a density of  $1.5 \times 10^6$  cells  $\text{mL}^{-1}$  and 10% GelMA hydrogels, crosslinked from 15 to 60 s for the following experiments.

### 3.2. Bioprinting of macroscale 3D cell-laden GelMA hydrogel constructs

We tested the ability of the modified bioprinting set up to create multiple cell-laden hydrogel constructs. Initially, 3D lattice designs were bioprinted by positioning parallel GelMA hydrogel fibers in one plane and stacking a second layer of perpendicular fibers on a plane above. Figure 7 shows representative fluorescent (figure 7(a)) and brightfield (figure 7(b)) images of these constructs. An additional application of bioprinters that has gained increasing attention in recent years is the formation of hydrogel microarrays [29–33]. Figure 7(d) shows that our bioprinting method may also be modified to form such arrays. However, for this application photopolymerization is performed after dots of hydrogel precursors are dispensed on a glass slide. In figure 7(e) we demonstrate that constructs can be fabricated with multiple architectures, including the MIT logo. Constructs with more complex architectures, such GelMA hydrogel blocks with impregnated planar and 3D bifurcating fiber networks (figures 7(f) and (g)), as well as hollow GelMA hydrogel fibers (figures 7(h) and (i)) may also be fabricated. Additional designs of macroscale constructs were fabricated from the bottom up by bioprinting stacked lines in close contact to one another, creating five stacked layers (figures 7(c) and (j)). Since

the bioprinting setup allowed for dispensing of individual fibers at a time and also permitted different hydrogels to be dispensed in the same construct, we alternated bioprinting of cell-laden GelMA fibers with printing of an agarose sacrificial fiber. The removal of the agarose fibers formed microchannels within the fabricated construct, as shown in higher magnification in figures 7(k) and (l). Bioprinting of multilayered constructs with embedded microchannels represents a feasible solution for vascularization of complex macroscale tissue constructs [34]. Viability data obtained from these constructs are shown in figure S3 (available from [stacks.iop.org/BF/6/024105/mmedia](http://stacks.iop.org/BF/6/024105/mmedia)) and demonstrate that even for larger constructs with five layers, at least  $\sim 75\%$  of the cells remained viable after the printing process.

These results demonstrate that one of the main advantages of direct-write bioprinting of photolabile cell-laden hydrogels is the ability to control macroscale architectures. Accordingly, the method we present allows for straightforward bioprinting of larger structures compared to recent ones fabricated via ink-jet [18, 29] or laser bioprinting [10]. Moreover, this method represents an important development from earlier direct-write printing of hydrogels used as seeding substrates to guide cellular arrangement [12, 14], since it allows for concomitant cell encapsulation and seeding. This represents an important development toward the fabrication of clinically relevant macroscale tissue constructs. Similarly, the potential for manipulation of the material properties of individual fibers and controlled positioning of different types of cells in the same construct represent additional advantages of the method described herein.

Limitations associated with this method, however, include the fact that the current system does not allow for dispensing of continuous fibers, different from other direct-write printers. However, fibers with lengths of up to 65 mm can be bioprinted at a time, which is sufficient to fabricate constructs measuring



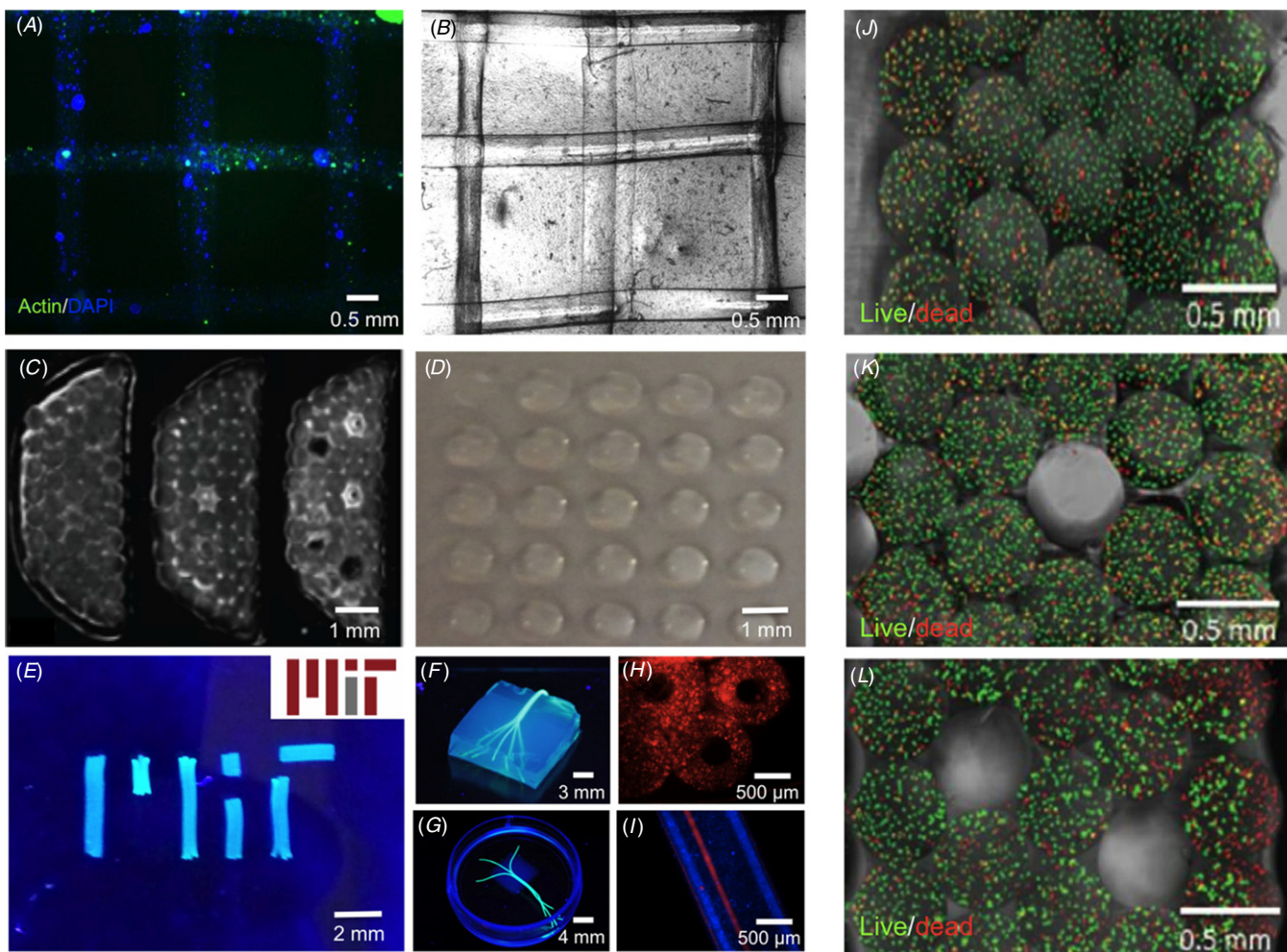


**Figure 7.** Different architectures biprinted with cell-laden GelMA hydrogels. (A) Fluorescence image of F-actin/DAPI stained two-layered lattice architecture biprinted with HepG2-laden GelMA hydrogels. (B) Representative brightfield image of lattice architecture shown in (A). (C) Cross-section images of five-layered stacked lines of NIH3T3 cell-laden hydrogels containing 0, 1 and 5 microchannels (left to right). (D) Photograph of hydrogel array biprinted with a HepG2-laden GelMA. (E) Photograph of MIT logo biprinted with fluorescent microbead-laden GelMA hydrogel fibers and actual MIT logo, for comparison (inset). (F), (G) Photograph of biprinted agarose hydrogel fibers replicating 3D branching networks embedded in GelMA hydrogel blocks. (H) Cross-section fluorescence image of microbead-laden hollow GelMA hydrogel fibers. (I) Longitudinal view of hollow fibers perfused with a red fluorescent dye. (J)–(L) Higher magnification of cross-sectional view of constructs shown in (C) stained for live and dead cells with 0 (J), 1 (K) and 5 (L) microchannels, respectively. The viability data for figures (J)–(L) are provided as supplementary information (figure S3 (available from [stacks.iop.org/BF/6/024105/mmedia](http://stacks.iop.org/BF/6/024105/mmedia))).

a few centimeters in size while maintaining cells viable for at least eight days. Furthermore, since the proposed method dispenses pre-polymerized cell-laden gels from a glass capillary one at a time, limitations recurrent to other printing methods, such as nozzle clogging, limited viscosity parameters associated with successful dispensing and stable gels, are overcome. Moreover, the requirement for a separate nozzle for biprinting different gels and cells in a same construct that is common in general direct-write printers is prevented here, since different types of gels and cells can be printed simply by alternating the ink vial. These represent further advantages of the proposed method when compared to existing direct-write printing of cell-laden materials.

### 3.3. Cell viability in biprinted cell-laden GelMA hydrogels

A common concern associated with printing of cells is whether the stress generated during the printing process may affect

cell viability [8]. To validate the concept that the biprinting process does not affect the health of cells encapsulated in GelMA hydrogels, we compared the ratio of live to dead cells in biprinted constructs versus control hydrogels fabricated via previously established methods [22] (figures 8(a)–(d)). Results from a viability assay at day 1 showed that biprinted cell-laden hydrogels photopolymerized for 60 s were associated with lower viability than gels photopolymerized for 15 ( $p < 0.01$ ) and 30 s ( $p < 0.0001$ ), a trend that was also observed for the non-printed control groups ( $p < 0.0001$  and  $p < 0.01$ , respectively) (figure 8(d)). On day 4, however, the biprinted groups had a higher percentage of live cells than the 60 s control group ( $p < 0.01$ ). On day 8 no significant differences were found between different groups (figure 8(d)). These results are consistent with the viability data observed for microfabricated cell-laden GelMA hydrogels presented in earlier reports [22, 25–27]. Overall, these results showed that cell viability

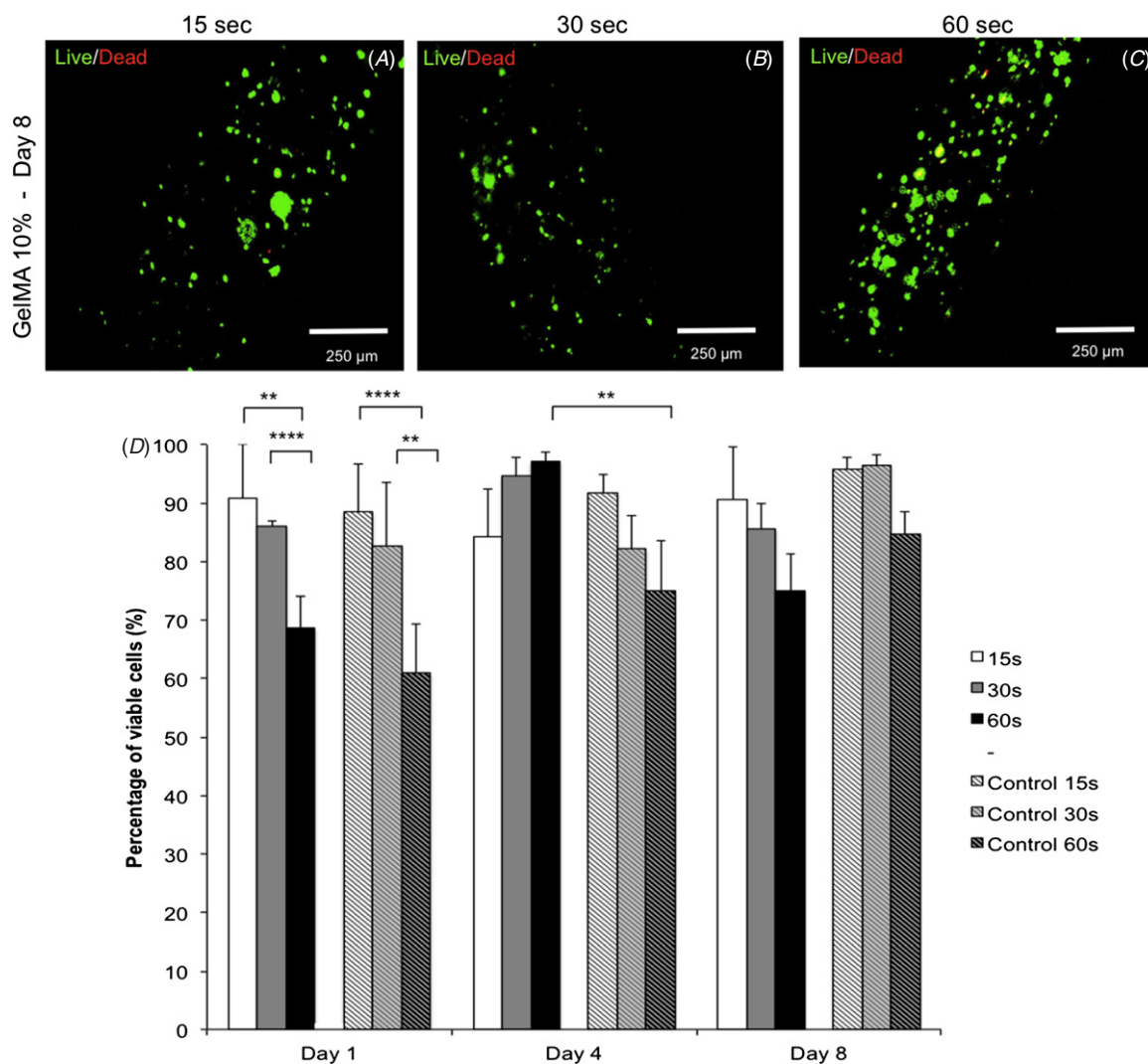


**Figure 8.** Viability of bioprinted HepG2-laden 10% GelMA hydrogels at different exposure times. Representative live/dead images from day 8 illustrating high HepG2 viability following (A) 15, (B) 30 and (C) 60 s of UV light exposure. (D) Quantitative data for cell viability in bioprinted cell-laden hydrogels at different UV light exposure times (\*\* $p < 0.01$ ; \*\*\*\* $p < 0.0001$ ).

could be preserved at levels higher than 80% for periods of at least eight days in bioprinted constructs. Additional images illustrating proliferation and spreading of NIH3T3s in bioprinted cell-laden GelMA hydrogels are shown in figure S5 (available from [stacks.iop.org/BF/6/024105/mmedia](http://stacks.iop.org/BF/6/024105/mmedia)). Moreover, early proliferation data obtained from bioprinted and control HepG2-laden GelMA hydrogels confirmed that the printing process did not affect the health of the encapsulated cells (figure S6 (available from [stacks.iop.org/BF/6/024105/mmedia](http://stacks.iop.org/BF/6/024105/mmedia))), since bioprinted constructs had higher proliferation rates than non-printed gels. This could be attributed to the easier access of cells to nutrients in bioprinted structures as compared to control hydrogel blocks, where the diffusion of media is limited. Although our results showed that a significant stress (load) was required to dispense the cell-laden hydrogels from the glass capillary, cell viability and proliferation were not significantly affected, therefore we suggest that the hydrogel matrix may function as barrier to protect the encapsulated cells from the shear stress resulting from friction with the capillary during dispensing. This ‘protective’ mechanism represents another

advantage of the current approach as compared to bioprinting of scaffold-free cell suspensions, such as occurring with inkjet bioprinters [8]. One of the current limitations of the proposed approach, however, is that cell viability is increasingly limited in larger constructs. This is primarily due to the fact that in larger constructs cells remain encapsulated in the hydrogel precursor without access to media for longer periods of time. One alternative that we had to adopt to preserve cell viability was to trypsinize and encapsulate cells immediately before bioprinting each layer. This allowed the cells to remain attached to the culture flasks and immersed in media for longer periods prior to the printing process.

#### 4. Conclusion

In summary, this work presents a strategy for direct-write bioprinting of cell-laden GelMA hydrogels. Our results show that cell-laden hydrogel constructs could be bioprinted with varying architectures, at multiple concentrations, mechanical properties and cell densities. Successful bioprinting was particularly correlated with the elastic modulus of the

hydrogels. Furthermore, results demonstrate that bioprinted constructs of HepG2-laden GelMA hydrogels retained high cell viability for at least eight days. Collectively, this work presents advancements toward bioprinting of complex cell-laden hydrogel tissue constructs.

## Acknowledgments

The authors acknowledge funding from National Institutes of Health (NIH-HL099073, AI081534, AR057837, DE021468, EB02597, GM095906) and the Presidential Early Career Award for Scientists and Engineers (PECASE) to AK. The authors gratefully acknowledge funding by the Defense Threat Reduction Agency (DTRA). The content is solely the responsibility of the authors and does not necessarily represent the official views of the awarding agency. Funding from the CNPq and the Sciences without Borders program is acknowledged by ALC and WAA. Finally, LEB acknowledges funding from the Australian Research Council (DP120104837). The authors also acknowledge Marat Sattarov, Rahul Anaadi Kurl and Aslihan Ekim for their help in the optimization of the system.

## References

- [1] Zorlutuna P *et al* 2012 Microfabricated biomaterials for engineering 3D tissues *Adv. Mater.* **24** 1782–804
- [2] Atala A, Bauer S B, Soker S, Yoo J J and Retik A B 2006 Tissue-engineered autologous bladders for patients needing cystoplasty *Lancet* **367** 1241–6
- [3] Carsin H, Ainaud P, Le Bever H, Rives J, Lakhel A, Stephanazzi J, Lambert F and Perrot J 2000 Cultured epithelial autografts in extensive burn coverage of severely traumatized patients: a five year single-center experience with 30 patients *Burns* **26** 379–87
- [4] Raya-Rivera A, Esquiliano D R, Yoo J J, Lopez-Bayghen E, Soker S and Atala A 2011 Tissue-engineered autologous urethras for patients who need reconstruction: an observational study *Lancet* **377** 1175–82
- [5] Warnke P H *et al* 2004 Growth and transplantation of a custom vascularised bone graft in a man *Lancet* **364** 766–70
- [6] Atala A, Kasper F K and Mikos A G 2012 Engineering complex tissues *Sci. Transl. Med.* **4** 1–10
- [7] Derby B 2012 Printing and prototyping of tissues and scaffolds *Science* **338** 921–6
- [8] Tasoglu S and Demirci U 2013 Bioprinting for stem cell research *Trends Biotechnol.* **31** 10–19
- [9] Guillemot F *et al* 2010 Laser-assisted cell printing: principle, physical parameters versus cell fate and perspectives in tissue engineering *Nanomedicine* **5** 507–15
- [10] Guillotin B 2010 Laser assisted bioprinting of engineered tissue with high cell density and microscale organization *Biomaterials* **31** 7250–6
- [11] Chang C C, Boland E D, Williams S K and Hoying J B 2011 Direct-write bioprinting three-dimensional biohybrid systems for future regenerative therapies *J. Biomed. Mater. Res. B* **98** 160–70
- [12] Hanson Shepherd J N, Parker S T, Shepherd R F, Gillette M U, Lewis J A and Nuzzo R G 2011 3D microperiodic hydrogel scaffolds for robust neuronal cultures *Adv. Funct. Mater.* **21** 47–54
- [13] Mannoor M S, Jiang Z, James T, Kong Y L, Malatesta K A, Soboyejo W O, Verma N, Gracias D H and McAlpine M C 2013 3D printed bionic ears *Nano Lett.* **13** 2634–9
- [14] Sun L, Parker S T, Syoji D, Wang X, Lewis J A and Kaplan D L 2012 Direct-write assembly of 3D silk/hydroxyapatite scaffolds for bone co-cultures *Adv. Healthc. Mater.* **1** 729–35
- [15] Skardal A, Zhang J, McCoard L, Xu X, Oottamasathien S and Prestwich G D 2010 Photocrosslinkable hyaluronan-gelatin hydrogels for two-step bioprinting *Tissue Eng. A* **16** 2675–85
- [16] Cui X and Boland T 2009 Human microvasculature fabrication using thermal inkjet printing technology *Biomaterials* **30** 6221–7
- [17] Miller E D, Li K, Kanade T, Weiss L E, Walker L M and Campbell P G 2011 Spatially directed guidance of stem cell population migration by immobilized patterns of growth factors *Biomaterials* **32** 2775–85
- [18] Xu T, Jin J, Gregory C, Hickman J J and Boland T 2005 Inkjet printing of viable mammalian cells *Biomaterials* **26** 93–99
- [19] Chahal D, Ahmadi A and Cheung K C 2012 Improving piezoelectric cell printing accuracy and reliability through neutral buoyancy of suspensions *Biotechnol. Bioeng.* **109** 2932–40
- [20] Xu T, Binder K W, Albanna M Z, Dice D, Zhao W, Yoo J J and Atala A 2013 Hybrid printing of mechanically and biologically improved constructs for cartilage tissue engineering applications *Biofabrication* **5** 015001
- [21] Moon S 2010 Layer by layer three-dimensional tissue epitaxy by cell-laden hydrogel droplets *Tissue Eng. C* **16** 157–66
- [22] Nichol J W, Koshy S T, Bae H, Hwang C M, Yamanlar S and Khademhosseini A 2010 Cell-laden microengineered gelatin methacrylate hydrogels *Biomaterials* **31** 5536–44
- [23] Ramon-Azcon J *et al* 2012 Gelatin methacrylate as a promising hydrogel for 3D microscale organization and proliferation of dielectrophoretically patterned cells *Lab. Chip* **12** 2959–69
- [24] Slaughter B V, Khurshid S S, Fisher A Z, Khademhosseini A and Peppas N A 2009 Hydrogels in regenerative medicine *Adv. Mater.* **21** 3307–29
- [25] Chen Y C, Lin R Z, Qi H, Yang Y, Bae H, Melero-Martin J M and Khademhosseini A 2012 Functional human vascular network generated in photocrosslinkable gelatin methacrylate hydrogels *Adv. Funct. Mater.* **22** 2027–39
- [26] Hutson C B, Nichol J W, Aubin H, Bae H, Yamanlar S, Al-Haque S, Koshy S T and Khademhosseini A 2011 Synthesis and characterization of tunable poly(ethylene glycol): gelatin methacrylate composite hydrogels *Tissue Eng. A* **17** 1713–23
- [27] Camci-Unal G, Cuttica D, Annabi N, Demarchi D and Khademhosseini A 2013 Synthesis and characterization of hybrid hyaluronic acid-gelatin hydrogels *Biomacromolecules* **14** 1085–92
- [28] DiFrancia C, Ward C T and Claus R O 1996 The single-fibre pull-out test: 1. Review and interpretation *Composites A* **27** 597–612
- [29] Matsusaki M, Sakaue K, Kadowaki K and Akashi M 2013 Three-dimensional human tissue chips fabricated by rapid and automatic inkjet cell printing *Adv. Healthc. Mater.* **2** 534–9
- [30] Ostrovidov S, Annabi N, Seidi A, Ramalingam M, Dehghani F, Kaji H and Khademhosseini A 2012 Controlled release of drugs from gradient hydrogels for high-throughput analysis of cell-drug interactions *Anal. Chem.* **84** 1302–9
- [31] Wu J, Wheelton I, Guo Y, Lu T, Du Y, Wang B, He J, Hu Y and Khademhosseini A 2011 A sandwiched microarray

- platform for benchtop cell-based high throughput screening *Biomaterials* **32** 841–8
- [32] Chung B G, Kang L and Khademhosseini A 2007 Micro- and nanoscale technologies for tissue engineering and drug discovery applications *Expert Opin. Drug Discov.* **2** 1653–68
- [33] Khademhosseini A, Langer R, Borenstein J and Vacanti J P 2006 Microscale technologies for tissue engineering and biology *Proc. Natl Acad. Sci. USA* **103** 2480–7
- [34] Bae H, Puranik A S, Gauvin R, Edalat F, Carrillo-Conde B, Peppas N A and Khademhosseini A 2012 Building vascular networks *Sci. Transl. Med.* **4** 1–5